# Design, Fabrication and Characterization of Scandium Aluminum Nitride Based Piezoelectric Micromachined Ultrasonic Transducers

Qi Wang, Yipeng Lu, Sergey Mishin, Yury Oshmyansky, David A. Horsley, *Member, IEEE*

***Abstract*—This paper presents the design, fabrication and characterization of piezoelectric micromachined ultrasound transducers (PMUT) based on scandium doped aluminum nitride ($Sc_xAl_{1-x}N$) thin films (x=20%). ScAlN thin film was prepared with a dual magnetron system and patterned by a reactive ion etching system utilizing chlorine-based chemistry with an etching rate of 160 nm/min. The film was characterized by X-ray diffraction (XRD) which indicated a crystalline structure expansion compared to pure AlN and a well-aligned ScAlN film. ScAlN PMUTs were fabricated by a 2-mask process based on cavity SOI wafers. ScAlN PMUTs with 50 µm and 40 µm diameter had a large dynamic displacement sensitivity measured in air of 25 nm/V at 17 MHz and 10 nm/V at 25 MHz, twice that of AlN PMUTs with the same dimensions. The peak displacement as a function of electrode coverage was characterized, with maximum displacement achieved with an electrode radius equal to 70% of the PMUT radius. Electrical impedance measurements indicated that the ScAlN PMUTs had 20% greater electromechanical coupling coefficient ($k_t^2$) compared to AlN PMUTs. The output pressure of a 7x7 ScAlN PMUT array was 0.7 kPa/V at ~1.7 mm away from the array, which is ~3 times greater that of an 8x8 AlN PMUT array with the same element geometry and fill factor measured at the same distance. Acoustic spreading loss and PMUT insertion loss from mechanical transmit to receive was characterized with a 15x15 ScAlN PMUT array via hydrophone and LDV.**

***Index Terms*—PMUT, piezoelectric films, piezoelectric transducers**

## I. INTRODUCTION

MANY applications have been developed based on micromachined ultrasonic transducers (MUTs) in recent years, such as medical imaging [1]–[3], gesture sensors [4], ultrasonic fingerprint sensors [5], and body-composition sensors [6]. MUTs have a better acoustic coupling, lower manufacturing cost and lower power consumption compared to conventional bulk ultrasonic transducers. Piezoelectric micromachined ultrasonic transducers (PMUT) have been rapidly developed in recent years due to the progress of piezoelectric thin films. Aluminum nitride (AlN) has been widely used for piezoelectric MEMS device fabrication because it is available from a number of MEMS foundries and is compatible with CMOS manufacturing [7]–[9]. However, compared to lead zirconate tianate (PZT), a piezoelectric material which requires high annealing temperature and is not process-compatible with CMOS, AlN has relatively low piezoelectric coefficient ($e_{31,f}$), which leads to low sensitivity and low electromechanical coupling ($k_t^2$) [9]-[11].

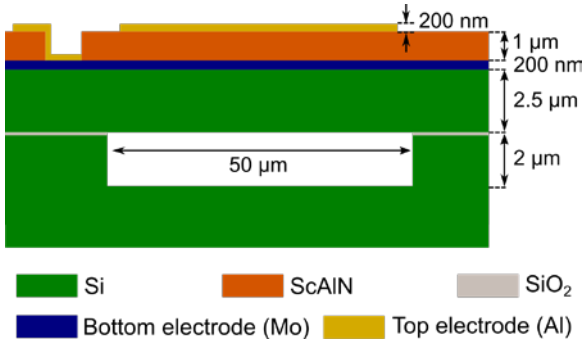

Fig. 1, Schematic cross-section of PMUT

Scandium (Sc) doping has been proposed recently as a means to increase the $e_{31,f}$ of AlN, while maintaining process compatibility with existing AlN based manufacturing [12]. Most of the previously-reported work on ScAlN focused on bulk acoustic wave (BAW) resonators or surface acoustic wave (SAW) devices which utilize the longitudinal piezoelectric mode and require high stiffness to achieve high frequency operation and high quality factor (Q) [12]-[13]. However, studies also found that with the increase of Sc doping concentrations, the stiffness of the thin film decreased and the dielectric constant increased [14]-[15]. In this paper, we present flexural PMUT devices which use the transverse piezoelectric mode and where the reduced stiffness of ScAlN may provide a benefit over conventional AlN.

This paragraph of the first footnote will contain the date on which you submitted your paper for review. It will also contain support information, including sponsor and financial support acknowledgment. For example, "This work was supported in part by the U.S. Department of Commerce under Grant BS123456".

The next few paragraphs should contain the authors' current affiliations, including current address and e-mail. For example, F. A. Author is with the National Institute of Standards and Technology, Boulder, CO 80305 USA (e-mail: author@ boulder.nist.gov).

S. B. Author, Jr., was with Rice University, Houston, TX 77005 USA. He is now with the Department of Physics, Colorado State University, Fort Collins, CO 80523 USA (e-mail: author@lamar.colostate.edu).

T. C. Author is with the Electrical Engineering Department, University of Colorado, Boulder, CO 80309 USA, on leave from the National Research Institute for Metals, Tsukuba, Japan (e-mail: author@nrim.go.jp).

TABLE I
RIE PARAMETERS

| Parameter | Values |
|---|---|
| $Cl_2$ flow rate (sccm) | 90 |
| $BCl_3$ flow rate (sccm) | 30 |
| He flow rate (sccm) | 100 |
| TCP RF Power (W) | 550 |
| RF Bias Power (W) | 150 |

## II. Materials and Methods

A cross-section schematic of a PMUT is shown in Fig. 1. The PMUT was composed of a 1 µm thick ScAlN piezoelectric layer, a 200 nm Mo layer as bottom electrode and a 2.5 µm thick silicon membrane. Devices were also fabricated using pure AlN with identical film thicknesses and geometries in order to provide a comparison between ScAlN and AlN PMUTs. The fabrication process used custom cavity SOI (CSOI) substrates wherein vacuum cavities are formed beneath the Si device layer of the CSOI wafer [10]. This process avoids the need for through-wafer etching or sacrificial release layers and eliminates the possible squeeze-film damping between the PMUT membrane and the Si substrate. 150 mm diameter CSOI wafers (IceMOS Technologies) were manufactured with 2 µm deep cavities patterned with diameters from 40 µm to 50 µm and both individual PMUTs and 2D arrays of PMUTs were defined on the wafer. A 7×49 array composed of PMUTs with 50 µm diameter and 70 µm pitch is shown in Fig. 2.

The Mo and $Sc_xAl_{1-x}N$ (x=20%) layers were sputtered in an Advanced Modular Systems (AMS) cluster tool with AlN deposition chambers and ion beam trimming module. The system used a standard dual conical magnetron with an AC deposition source operating at 40 kHz and power varying from 3 to 10 kW. The ScAlN deposition process was in deep poison mode using targets composed of Al and Sc pieces. Compared to Al-Sc alloy target and multiple targets of Al and Sc, multiple piece targets are easy to make and practical for high volume production. Locally adjusted magnetic field for target pieces of both Al and Sc guaranteed a constant thin film composition over the entire target life. Substrate rotation was utilized to compensate for the variation of the sputtering yield for different materials and composition non-uniformity across the substrate.

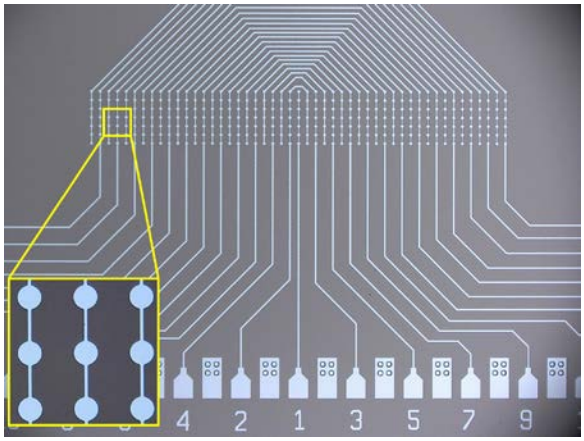

Fig. 2, An optical microscope image of a 7x49 PMUT array. The individual PMUTs are 50 µm diameter and the array pitch is 70 µm.

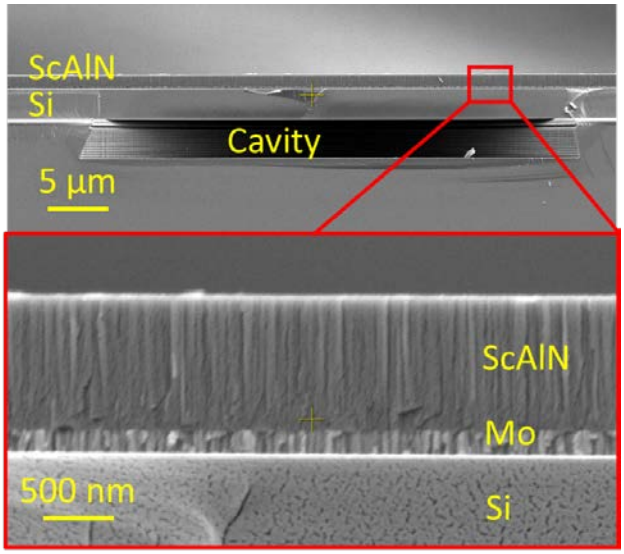

Fig. 3, Cross-sectional SEM image of a ScAlN PMUT. The Mo and ScAlN show good columnar structure indicating a highly c-axis oriented film.

The CSOI wafers were cleaned by ion milling first in order to achieve a good interface for the following thin film deposition. A 30 nm thick ScAlN film was first deposited on the CSOI as a seed layer in order to achieve a good crystalline structure of the subsequent Mo and ScAlN layers. Then a 200 nm thick molybdenum (Mo) layer was sputtered as the bottom electrode in a different chamber in the system without breaking vacuum. Finally, 1 µm thick ScAlN was sputtered on the Mo layer. A cross-section scanning electron microscope (SEM) image of a PMUT, Fig. 3, shows the dense columnar structure of the ScAlN film and Mo bottom electrode.

Following deposition of the ScAlN layer, vias were opened to contact the Mo bottom electrode. AlN films are often etched using heated Microposit MF-319, a positive photoresist developer mainly composed of tetramethylammonium hydroxide (TMAH). However, experiments showed that the ScAlN etch rate in MF-319 was ~50 nm/min at 60 °C to 70°C, approximately 4 times slower than that of AlN thin films at the same etching temperature. For this reason, reactive ion etching (RIE) in a transformer coupled plasma (TCP) etcher was studied using a combination of $Cl_2$ and $BCl_3$ gases with He used as diluent to improve etch uniformity. A 6.5 µm thick g-line photoresist (OCG 825 35S, Fujifilm) was spin coated, patterned, and hard baked for 16 hours to be used as a mask. An etch rate of 160 nm/min was achieved with the recipe shown in the Table 1 with an etching selectivity of 0.4 to the mask. Following the via etch, a 200 nm thick aluminum (Al) layer was evaporated and patterned by a lift-off process to form the top electrode and contact pads for the top and bottom electrodes.

## III. Results

### A. ScAlN film characterization

The ScAlN crystalline structure was studied using X-ray diffraction (XRD). Fig. 4(a) shows a comparison of the XRD peaks of pure AlN and ScAlN thin films on Mo electrode with

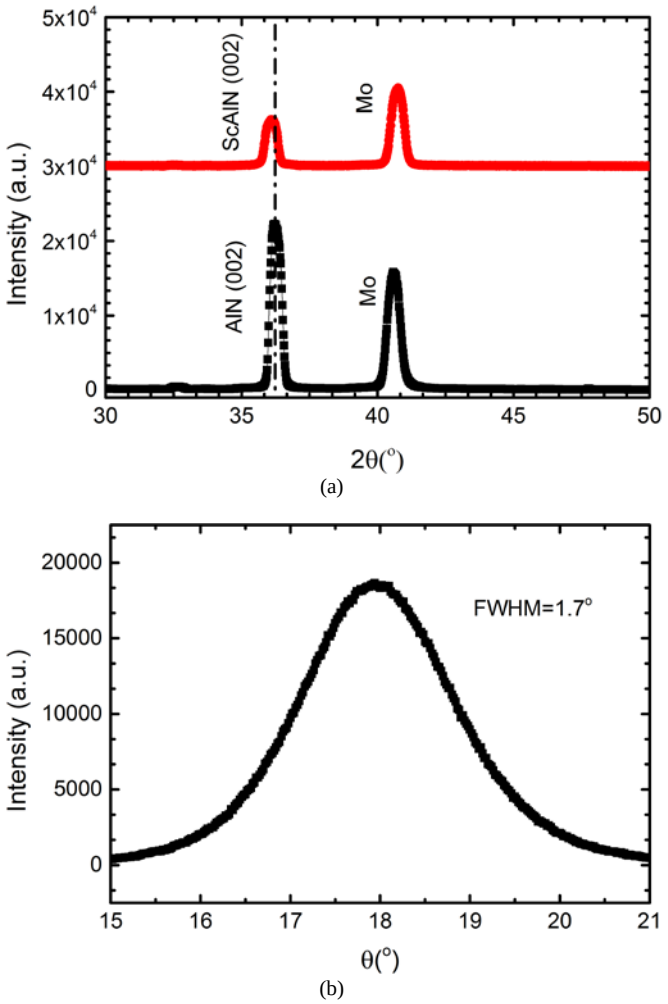


Fig. 4, (a) Normal coupled XRD measurement of ScAlN and AlN films; (b) Rocking curve measurement of the ScAlN (002) peak.

1 µm thickness. The (002) peak of ScAlN was shifted to a slightly lower angle compared with that of AlN, indicating an expansion of the crystalline lattice according to Bragg's law. The rocking curve of the ScAlN (002) peak was also measured and is shown in Fig. 4(b). The full-width-half-maximum (FWHM) of the peak is 1.7°, indicating that the c-axis of the ScAlN thin film is well aligned and predicting good piezoelectric properties.

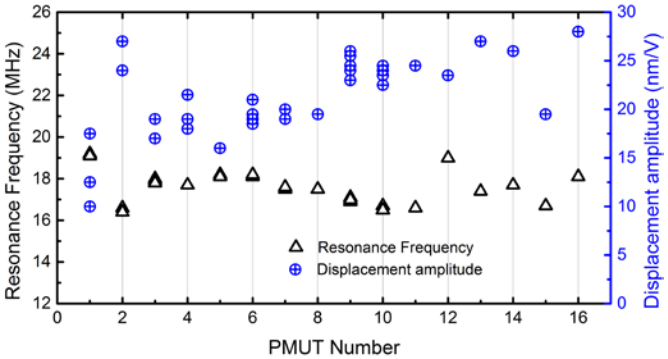


Fig. 5, Measured resonance frequency and dynamic displacement at resonance for ScAlN PMUT with 50 m diameter and 2.5 m nominal Si thickness.

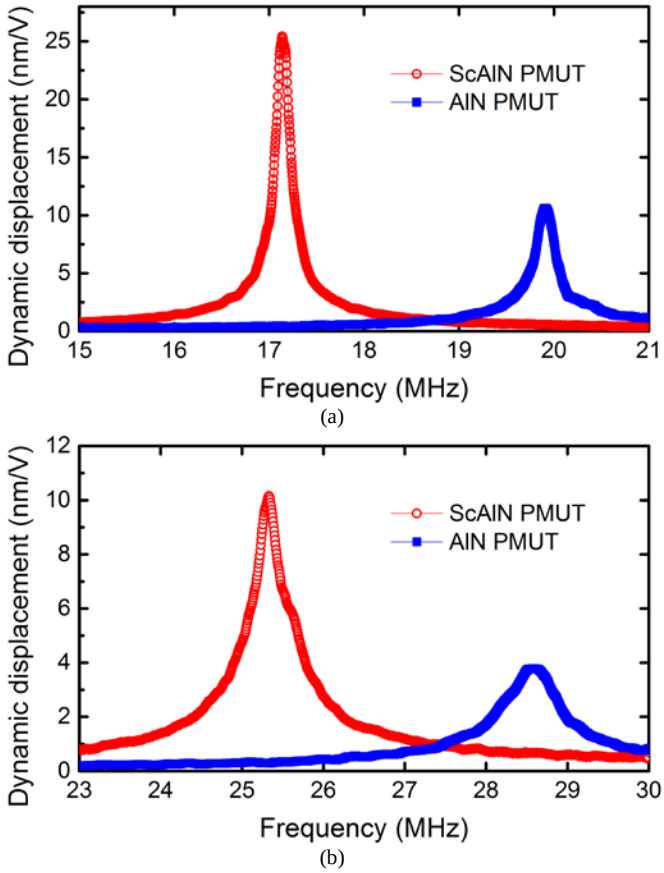


Fig. 6, LDV measurement results for (a) 50 µm diameter and (b) 40 µm diameter ScAlN and AlN PMUTs.

### *B. Dynamic characterization*

The frequency response of ScAlN PMUTs and AlN PMUTs with the same geometry were tested in air using a laser Doppler vibrometer (LDV, OFV 512 and OFV 2700, Polytec) in conjunction with a network analyzer (E5061B, Agilent Technology). LDV measurements were collected on 16 ScAlN PMUTs with 50 µm diameter selected from locations across one wafer, resulting in a 17.5 ± 1.5 MHz natural frequency, 22±4 nm/V peak displacement sensitivity at resonance, and an average quality factor of $Q$ = 140 in air. The die to die variation in resonant frequency was within 10% and the variation in amplitude was ~20%. The results are shown in Fig. 5. Cross-section SEM images showed that the Si thickness of these samples varied from 2.40 µm to 2.93 µm. Fig. 6 compares the LDV results of ScAlN and AlN PMUTs with 50 µm diameter and 40 µm diameter. The peak displacement of the ScAlN PMUTs are more than two times as large as that of the AlN devices.

The difference in the resonance frequency of ScAlN and AlN PMUTs is due to the stiffness reduction from Sc doping. The resonant frequency of a circular PMUT can be computed from

$$f = \frac{1.63}{r^2}\sqrt{\frac{D}{\sum \rho_i t_i}} \quad (1)$$

where $r$ is the PMUT radius, $D$ is rigidity, $\rho$ and $t$ are the density and thickness of the Si, Mo, and ScAlN layers. The rigidity $D$ can be expressed as

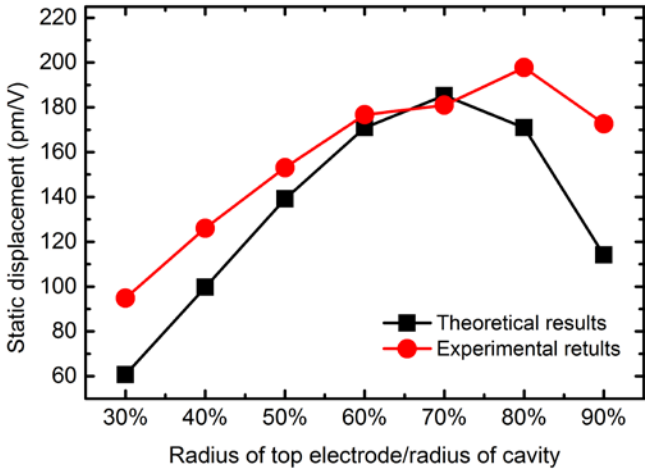


Fig. 7, Theoretical and experimental results of PMUT static displacement with different electrode radius

$$D = \frac{1}{3}\sum_{i=1}^{n}\frac{E_i^2(z_i^3 - z_{i-1}^3)}{1-\upsilon_i^2} \quad (2)$$

where $E_i$ is the Young's modulus and $v_i$ is the Poisson's ratio of the material, $z_i$ is the distance of the $i$-th layer top surface from the neutral axis. Using (1), the Young's modulus of ScAlN was estimated to be 200 GPa, which is consistent with the reported values obtained from ScAlN BAW devices with similar Sc composition [16]. This formula also confirms that the measured variation in natural frequency across the wafer is consistent with the measured variation of the Si device layer thickness.

To extract an estimate of the transverse thin-film piezoelectric coefficient ($e_{31,f}$) from the frequency response data, we normalized the peak displacement by the quality factor, yielding an average value of $d_s = d_p/Q = 180$ pm/V. $d_s$ is related to the transverse piezoelectric coefficient $e_{31,f}$ via [17]:

$$d_s = -r^2\frac{e_{31,f}(t_{si} + t_m + \frac{t_p}{2} - z_n)\cdot I_p(r)}{D\cdot I_d} \quad (3)$$

where $t_{si}$ is the thickness of Si substrate, $t_m$ is the thickness of bottom electrode, $t_p$ is the thickness of ScAlN film, $z_n$ is the distance from the middle of the ScAlN film to neutral axis, and $I_p(r)$ and $I_d$ are integrals related to the piezoelectric bending moment and modal stiffness of the PMUT, both of which depend on the assumed vibration mode shape of the PMUT, $u(r)$,

$$I_p(r_e) = \int_0^{r_e}(r_e\frac{d^2u(r_e)}{dr_e^2} + \frac{du(r_e)}{dr_e})\cdot dr_e \quad (4)$$

$$I_d = \int_0^1[(\frac{d^2u(r)}{dr^2} + \frac{1}{r}\frac{du(r)}{dr})^2 - 2(1-\upsilon)\frac{1}{r}\frac{du(r)}{dr}\frac{d^2u(r)}{dr^2}]rdr \quad (5)$$

where $\upsilon$ is Poisson's ratio. $I_p(r_e)$ is a function of $r_e$, the radius of the circular top electrode normalized to the PMUT radius. Using $u(r) = (1-r^2)^2$ as the assumed mode shape for the 01 vibration mode of a circular membrane, (4) yields $I_p = -1$ at $r_e = 70\%$ and $I_d = 10.67$. Substituting these values along with the geometrical parameters into (3) yields an estimate of $e_{31,f}$ ~1.6 C/m$^2$ which is ~60% higher than that of AlN.

Equation (3) also allows the optimum electrode radius for peak displacement to be identified. The estimated material properties including Young's modulus and $e_{31,f}$ were used in (3) to compute the theoretical displacement with $r_e$ varying from 30% to 90%. The results are compared to experimental measurements of PMUTs with varying electrode diameters in Fig. 7, demonstrating good agreement between model and experiment, with the maximum displacement observed with electrode radius from 70% to 80% of the PMUT radius.

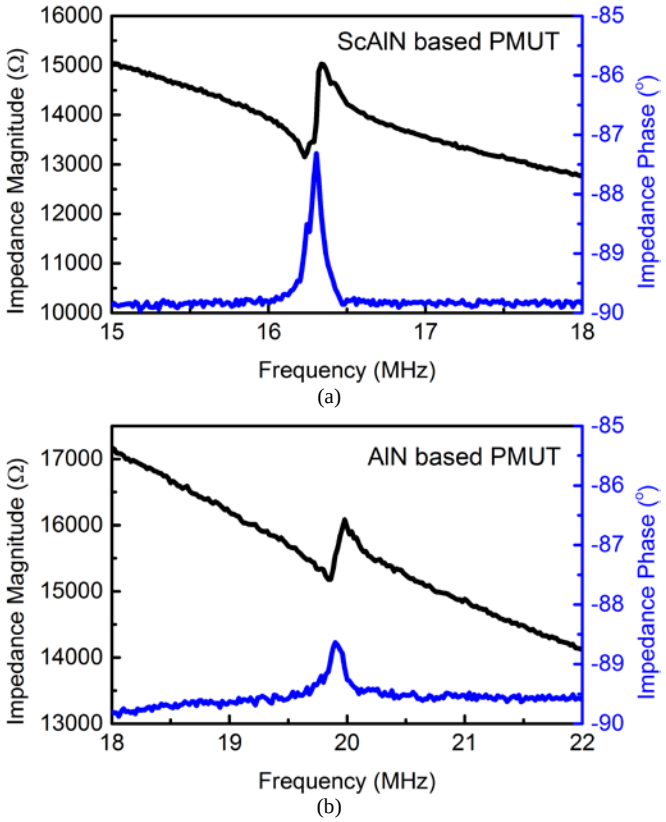


Fig. 8, Impedance measurement results for 50 μm diameter (a) ScAlN PMUT and (b) AlN PMUT

### C. *Electrical characterization*

Impedance measurements of ScAlN and AlN PMUTs, Fig. 8, were performed in air using a GSG RF probe calibrated with an impedance substrate standard (Cascade Microtech). The electromechanical coupling factor $k_t^2$ was calculated by:

$$k_t^2 = \frac{\pi^2}{4}\frac{f_r}{f_a}\frac{f_a - f_r}{f_a} \quad (6)$$

where $f_a$ and $f_r$ are the anti-resonant and resonant frequency respectively. $k_t^2$ was 1.8% for ScAlN PMUTs, 20% higher compared to the AlN PMUT's 1.47% which was close to the value expected for a pure AlN device using the 31 piezo coefficient. The relative dielectric permittivity ($\varepsilon_{ScAlN}$) of ScAlN was also estimated from the impedance test as ~12 which is around 20% higher than that of pure AlN. The estimated dielectric permittivity is consistent with the value reported in [12].

A figure of merit for comparing piezoelectric materials for PMUTs is the 31 electromechanical coupling coefficient, $k_{31}^2 \propto e_{31,f}^2/\varepsilon_{33}$ [18]-[19]. For pulse-echo performance, this metric can be interpreted as follows – the square of the piezocoefficient appears in the numerator because both the TX and RX operations require energy conversion between the electrical and

TABLE II
COMPARISON OF PIEZOELECTRIC MATERIAL PROPERTIES

| Materials | $e_{31,f}$ (C/m$^2$) | $\varepsilon_{33}$ | $E$ (GPa) | $\frac{e_{31,f}^2}{\varepsilon_{33}\varepsilon_{33}}$ (GPa) |
|---|---|---|---|---|
| PZT [17] | -14.0 | 1200 | 65 | 18.5 |
| AlN [17] | -1.05 | 10.5 | 390 | 10.8 |
| ScAlN (this work) | -1.6 | 12 | 200 | 24.1 |

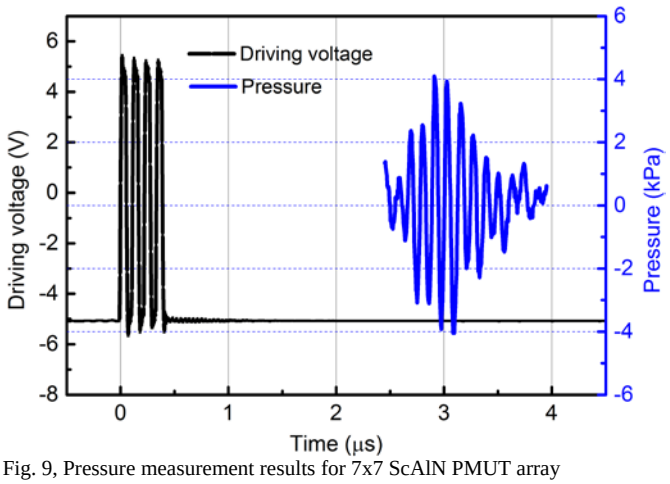

Fig. 9, Pressure measurement results for 7x7 ScAlN PMUT array

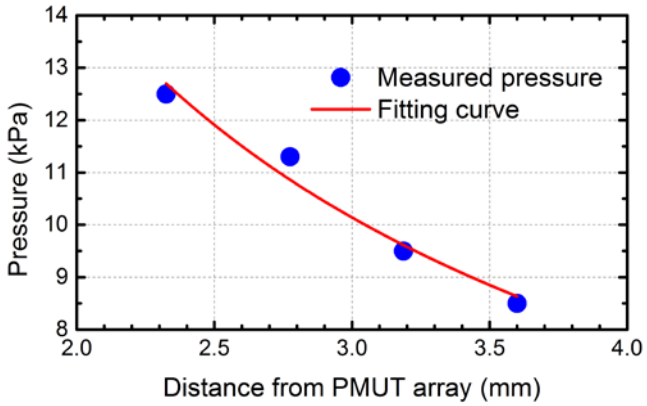

Fig. 10, Acoustic pressure measured from a 15x15 PMUT array

mechanical domains, while the dielectric constant is in the denominator because the RX charge is converted to a voltage by dividing by the capacitance. AlN, ScAlN, and PZT are compared in Table II using the extracted material parameters reported here. Note that while PZT is superior to AlN, the figure-of-merit for ScAlN is 30% greater than that of PZT. One caveat to this conclusion is that the presence of parasitic capacitance (e.g. due to bond-pads or cables between the PMUT and the receive amplifier) will greatly degrade the RX signal amplitude of a ScAlN or AlN PMUT due to the much lower dielectric constant of these materials. For example, a 50 μm diameter PMUT with $r_e$ = 70% and a 1 μm thick ScAlN layer has a capacitance of 0.1 pF, so the presence of a 1 pF bond-pad capacitance will reduce the RX voltage by a factor of 11 (= 0.1 pF /1.1 pF). In comparison, a PZT PMUT of the same size has 100 times greater capacitance, so a 1 pF parasitic capacitance would have negligible effect on the RX voltage.

### *D. Acoustic characterization*

An array of ScAlN PMUTs was immersed in non-conductive fluid (Fluorinert FC-70, 3M) and the output acoustic pressure was measured with a 70 μm diameter needle hydrophone (Precision Acoustic, Inc.). The results are shown in Fig. 9. A 7x7 ScAlN PMUT array was driven by four 9 MHz 11 Vpp pulses from a function generator (Rigol, DG-4102). The measured pressure generated by the ScAlN PMUT array was

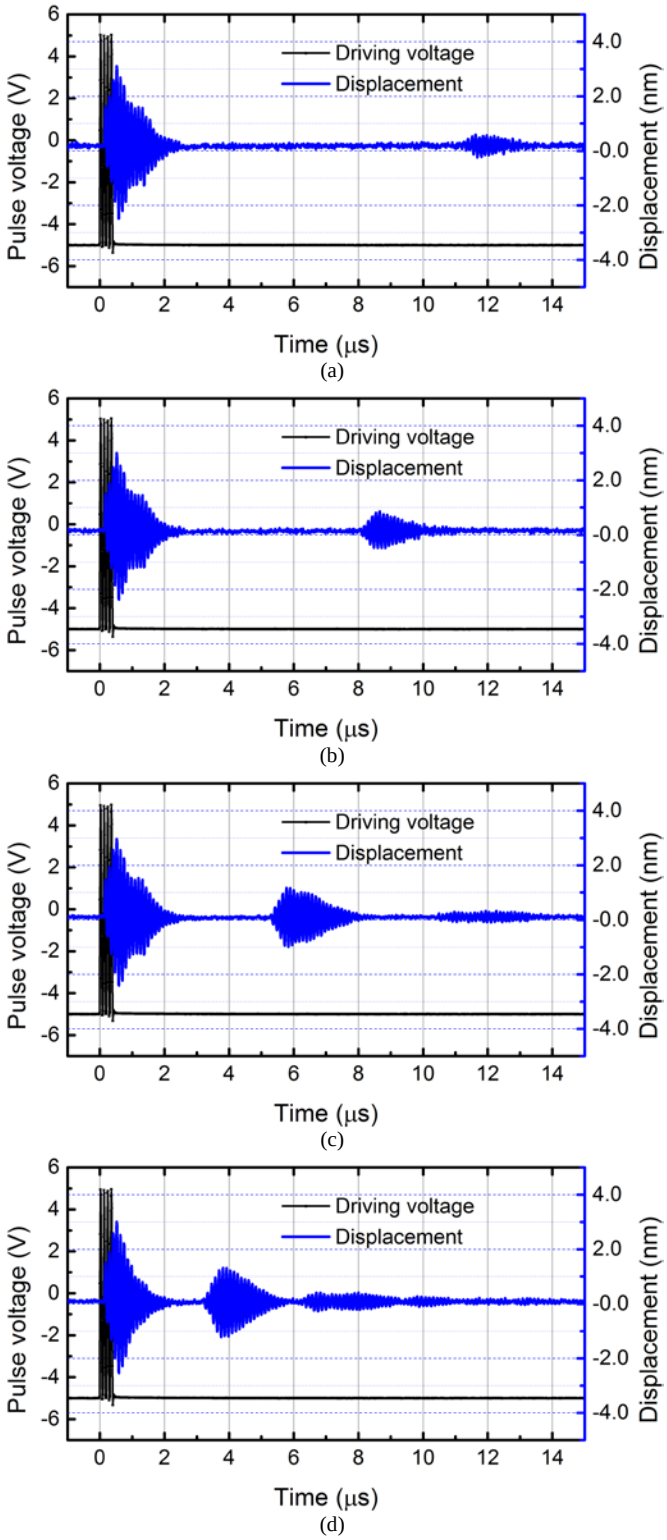

Fig. 11, LDV measurement of pulse-echo from a ScAlN PMUT in the center of 15x15 array with different Fluorinert heights of 4 mm, 3 mm, 2 mm and 1.2 mm.

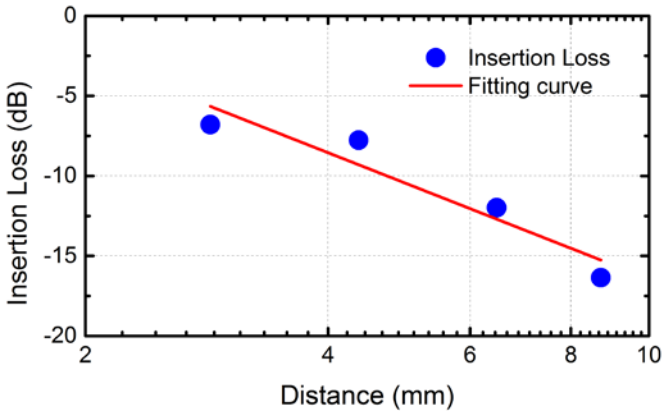


Fig. 12. Measured insertion loss from TX to RX vibration amplitudes as a function of round-trip pulse-echo distance.

detected at ~2.5 µs after the pulse generation, which corresponds to ~1.7 mm from the PMUT surface to the hydrophone. The peak-to-peak pressure detected was ~8 kPa, which was 30% larger than ~6 kPa pressure generated from a 8x8 AlN PMUT array driven at 25 Vpp, suggesting 3x greater transmit efficiency from the ScAlN array.

The output acoustic pressure of a 15x15 ScAlN PMUT array was measured via hydrophone at different distances to PMUT surface. The measured peak-to-peak pressure versus distance is shown in Fig. 10. The result shows that the pressure decays inversely with the radial distance from the array [20]:

$$P(r) = P_0 R_0 x^{-1} \quad (7)$$

where $R_0$ is the Rayleigh distance and $P_0$ is the theoretical surface pressure. A fit of (7) to the experimental data gives $R_0$ = 2.9 mm and $P_0$ = 20.6 kPa. Given that the peak-to-peak displacement is 5 nm, the value of $P_0$ gives a transmit sensitivity of $S_{TX}$ = 4 kPa/nm.

The dynamic displacement of a 15x15 ScAlN PMUT array driven with 11 Vpp and immersed in fluid was measured via LDV, Fig. 11. An ~5 nm displacement of the center ScAlN PMUT was measured during the transmit (TX) excitation. PMUT vibration due to received (RX) echoes returning from the fluid-air surface were also visible in these experiments. The Fluorinert-air surface was varied from 4 mm to 1.2 mm, and the plots in Fig. 11 show the echoes return 11 µs, 8 µs, 5 µs and 3 µs after the TX pulse is sent. The corresponding round-trip distances calculated from these pulse echo measurements are consistent with the Fluorinert height using $c$ = 750 m/s as the speed of sound in Fluorinert. In Fig. 11(c) and (d), a second echo can be observed due to the short liquid distance and large output pressure. The vibration amplitude of the first received echo relative to the transmit vibration amplitude fits the acoustic spreading model from (7),

$$d_{RX}(x)/d_{TX} = R_0 x^{-1} \quad (8)$$

This model is plotted along with the experimental data in dB units in Fig. 12. Comparing the experimental pressure measurements from Fig. 10 with the RX vibration amplitudes shown in Fig. 11, the receive sensitivity of the array is estimated to be $S_{RX}$ = 0.25 nm/kPa. Since the PMUT is a reciprocal transducer, $S_{TX}$=$S_{RX}^{-1}$, as expected.

## IV. CONCLUSION

The results presented here demonstrate that ScAlN PMUTs have better performance than PMUTs made with AlN. Using 20% Sc, the transmit amplitude was increased by a factor of two relative to PMUTs made with pure AlN, consistent with a 60% increase in the transverse piezoelectric coefficient, $e_{31,f}$. The PMUT fabrication process is nearly unchanged by introducing ScAlN. While wet etching of $Sc_{0.2}Al_{0.8}N$ in TMAH proceeds at a much slower etch rate than pure AlN, a $Cl_2/BCl_3$ plasma etch was demonstrated to achieve an etch rate of 120 nm/min for $Sc_{0.2}Al_{0.8}N$. We expect that increasing the Sc concentration would further improve PMUT performance, since other work has shown that the piezoelectric coefficients of ScAlN increase as the Sc concentration is increased up to 40%. While RF devices, such as BAW filters, may suffer due to the reduced stiffness (and therefore lower acoustic velocity) that occurs as the Sc concentration is increased, this reduced stiffness does not degrade the performance of PMUTs.

## ACKNOWLEDGMENT

The authors thank UC Berkeley Marvel Nanolab for the advice and help on the fabrication process, Berkeley Sensor and Actuator (BSAC) industrial members for financial support, and IceMOS Technology for providing cavity SOI wafers.

## REFERENCES

[1] Qi Wang *et al.*, "Scandium doped aluminum nitride based piezoelectric micromachined ultrasound transducers," in *Proc. of Solid-State Sensors, Actuators and Microsystems Work Shop*, Hilton Head, South Carolina, 2016, pp. 436–439.

[2] D. E. Dausch, K. H. Gilchrist, J. B. Carlson, S. D. Hall, J. B. Castellucci, and O. T. von Ramm, "In vivo real-time 3-D intracardiac echo using PMUT arrays," *IEEE Trans. Ultrason. Ferroelectr. Freq. Control*, vol. 61, no. 10, pp. 1754–1764, Oct. 2014.

[3] Y. Lu *et al.*, "Waveguide piezoelectric micromachined ultrasonic transducer array for short-range pulse-echo imaging," *Appl. Phys. Lett.*, vol. 106, no. 19, p. 193506, May 2015.

[4] R. J. Przybyla, H. Y. Tang, S. E. Shelton, D. A. Horsley, and B. E. Boser, "12.1 3D ultrasonic gesture recognition," in *2014 IEEE International Solid-State Circuits Conference Digest of Technical Papers (ISSCC)*, 2014, pp. 210–211.

[5] Y. Lu *et al.*, "Ultrasonic fingerprint sensor using a piezoelectric micromachined ultrasonic transducer array integrated with complementary metal oxide semiconductor electronics," *Appl. Phys. Lett.*, vol. 106, no. 26, p. 263503, Jun. 2015.

[6] H.-Y. Tang, Y. Lu, S. Fung, D. A. Horsley, and B. E. Boser, "11.8 Integrated ultrasonic system for measuring body-fat composition," in *Solid- State Circuits Conference - (ISSCC), 2015 IEEE International*, 2015, pp. 1–3.

[7] D. A. Horsley *et al.*, "Piezoelectric micromachined ultrasonic transducers in consumer electronics: The next little thing?," in *2016 IEEE 29th International Conference on Micro Electro Mechanical Systems (MEMS)*, 2016, pp. 145–148.

[8] R. Ruby and P. Merchant, "Micromachined thin film bulk acoustic resonators," in *Frequency Control Symposium, 1994. 48th., Proceedings of the 1994 IEEE International*, 1994, pp. 135–138.

[9] J. Zou, C.-M. Lin, Y.-Y. Chen, and A. P. Pisano, “Theoretical study of thermally stable SiO2/AlN/SiO2 Lamb wave resonators at high temperatures,” *J. Appl. Phys.*, vol. 115, no. 9, p. 94510, Mar. 2014.

[10] Y. Lu and D. A. Horsley, “Modeling, Fabrication, and Characterization of Piezoelectric Micromachined Ultrasonic Transducer Arrays Based on Cavity SOI Wafers,” *J. Microelectromechanical Syst.*, vol. 24, no. 4, pp. 1142–1149, Aug. 2015.

[11] Q. Wang, H. Oguchi, M. Hara, and H. Kuwano, “Investigation of dominant factors to control c-axis tilt angle of aln thin films for efficient energy harvesting,” in *2014 IEEE 27th International Conference on Micro Electro Mechanical Systems (MEMS)*, 2014, pp. 636–639.

[12] R. Matloub *et al.*, “Piezoelectric Al1−xScxN thin films: A semiconductor compatible solution for mechanical energy harvesting and sensors,” *Appl. Phys. Lett.*, vol. 102, no. 15, p. 152903, Apr. 2013.

[13] M. Moreira, J. Bjurström, I. Katardjev, and V. Yantchev, “Aluminum scandium nitride thin-film bulk acoustic resonators for wide band applications,” *Vacuum*, vol. 86, no. 1, pp. 23–26, Jul. 2011.

[14] K. Hashimoto, S. Sato, A. Teshigahara, T. Nakamura, and K. Kano, “High-performance surface acoustic wave resonators in the 1 to 3 GHz range using a ScAlN/6H-SiC structure,” *IEEE Trans. Ultrason. Ferroelectr. Freq. Control*, vol. 60, no. 3, pp. 637–642, Mar. 2013.

[15] A. Konno *et al.*, “Determination of full material constants of ScAlN thin film from bulk and leaky Lamb waves in MEMS-based samples,” in *2014 IEEE International Ultrasonics Symposium*, 2014, pp. 273–276.

[16] K. Umeda, H. Kawai, A. Honda, M. Akiyama, T. Kato, and T. Fukura, “Piezoelectric properties of ScAlN thin films for piezo-MEMS devices,” in *2013 IEEE 26th International Conference on Micro Electro Mechanical Systems (MEMS)*, 2013, pp. 733–736.

[17] M. Dubois and P. Muralt, “PZT thin film actuated elastic fin micromotor,” *IEEE Trans. Ultrason. Ferroelectr. Freq. Control*, vol. 45, no. 5, pp. 1169–1177, Sep. 1998.

[18] P. Muralt and J. Baborowski, “Micromachined Ultrasonic Transducers and Acoustic Sensors Based on Piezoelectric Thin Films,” *J. Electroceramics*, vol. 12, no. 1–2, pp. 101–108.

[19] K. Smyth and S.-G. Kim, “Experiment and simulation validated analytical equivalent circuit model for piezoelectric micromachined ultrasonic transducers,” *IEEE Trans. Ultrason. Ferroelectr. Freq. Control*, vol. 62, no. 4, pp. 744–765, Apr. 2015.

[20] D. T. Blackstock, *Fundamentals of Physical Acoustics*. John Wiley & Sons, 2000.